Estrogen Treatment Prevents Gray Matter Atrophy in Experimental Autoimmune Encephalomyelitis

Allan J. MacKenzie-Graham,[1,2]★ **Gilda A. Rinek,**[1] **Andrea Avedisian,**[1]
Laurie B. Morales,[2] **Elizabeth Umeda,**[2] **Benoit Boulat,**[3] **Russell E. Jacobs,**[3]
Arthur W. Toga,[4] **and Rhonda R. Voskuhl**[2]

[1]Ahmanson-Lovelace Brain Mapping Center, Department of Neurology, University of California,
Los Angeles, Los Angeles, California
[2]Multiple Sclerosis Program, Department of Neurology, University of California, Los Angeles,
Los Angeles, California
[3]Beckman Institute, California Institute of Technology, Pasadena, California
[4]Laboratory of Neuroimaging, Department of Neurology, University of California, Los Angeles,
Los Angeles, California

Gray matter atrophy is an important correlate to clinical disability in multiple sclerosis (MS), and many treatment trials include atrophy as an outcome measure. Atrophy has been shown to occur in experimental autoimmune encephalomyelitis (EAE), the most commonly used animal model of MS. The clinical severity of EAE is reduced in estrogen-reated mice, but it remains unknown whether estrogen treatment can reduce gray matter atrophy in EAE. In this study, mice with EAE were treated with either estrogen receptor (ER)-α ligand or ER-β ligand, and diffusion tensor images (DTI) were collected and neuropathology was performed. DTI showed atrophy in the cerebellar gray matter of vehicle-treated EAE mice compared with healthy controls but not in ER-α or ER-β ligand-treated EAE mice. Neuropathology demonstrated that Purkinje cell numbers were decreased in vehicle-treated EAE mice, whereas neither ER ligand-treated EAE groups showed a decrease. This is the first report of a neuroprotective therapy in EAE that unambiguously prevents gray matter atrophy while sparing a major neuronal cell type. Fractional anisotropy (FA) in the cerebellar white matter was decreased in vehicle- and ER-β ligand-treated but not in ER-α ligand-treated EAE mice. Inflammatory cell infiltration was increased in vehicle- and ER-β ligand-treated but not in ER-α ligand-treated EAE mice. Myelin staining was decreased in vehicle-treated EAE mice and was spared in both ER ligand-treated groups. This is consistent with decreased FA as a potential biomarker for inflammation rather than myelination or axonal damage in the cerebellum in EAE.   © 2012 Wiley Periodicals, Inc.

Key words: DTI; multiple sclerosis; mouse; ligand

Magnetic resonance imaging (MRI) measures of gray matter atrophy are an important characteristic of many neurodegenerative diseases, such as Alzheimer's disease, Parkinson's disease, and multiple sclerosis (MS).

In fact, there is a strong link between gray matter atrophy and disability in all of these diseases (Chard et al., 2002; Camicioli et al., 2003; Firbank et al., 2007). Whole-brain atrophy was described in MS over a decade ago (Rudick et al., 1999), and several studies have since demonstrated a strong relationship between gray matter atrophy and disability (Ge et al., 2000; Amato et al., 2008; Calabrese et al., 2010). Indeed, gray matter atrophy is considered to be one of the most clinically relevant markers of MS disease progression (Fisher et al., 2002; Bermel and Bakshi, 2006; van den Elskamp et al., 2010).

Diffusion tensor imaging (DTI) measures the diffusion of water molecules. When the mobility of a water molecule is not the same in all directions, its diffusion is said to be anisotropic. Anisotropic diffusion in the brain is due to underlying tissue anisotropy, with both myelin and axons contributing to the restriction of the free diffusion of water. Diffusion anisotropy is typically represented by

an anisotropy index such as the fractional anisotropy (FA), the fraction of the ''magnitude'' of the diffusion along the principal axis of the diffusion tensor (Pierpaoli and Basser, 1996). FA has been used as a marker for white matter tract integrity (Werring et al., 1999; Bammer et al., 2000; Filippi et al., 2001), reflecting the state of inflammation or myelination. Furthermore, it has been proposed that changes in the eigenvalues of the diffusion tensor may reflect either demyelination or axonal damage (Song et al., 2003; Budde et al., 2009).

MS relapses decrease during late pregnancy and increase after birth, when female sex hormones are at high and low levels, respectively (Birk et al., 1990; Confavreux et al., 1998), suggesting a protective role (Voskuhl, 2003). In experimental autoimmune encephalomyelitis (EAE), both estriol and estradiol have been shown to be protective (Jansson et al., 1994; Kim et al., 1999; Bebo et al., 2001; Liu et al., 2003; Palaszynski et al., 2004; Polanczyk et al., 2004; Papenfuss et al., 2011). Numerous anti-inflammatory mechanisms appear to underlie the protective effect of estrogen in EAE (Ito et al., 2001; Zang et al., 2002; Subramanian et al., 2003). Furthermore, work by our group has suggested a direct neuroprotective role for estrogens independent of these anti-inflammatory effects (Tiwari-Woodruff et al., 2007; Crawford et al., 2010; Spence et al., 2011).

The actions of estrogen are mediated primarily by nuclear estrogen receptor (ER)-α and ER-β, although nongenomic membrane effects have also been described (Weiss and Gurpide, 1988). Among the unresolved issues in the use of estrogens as neuroprotective agents is whether neuroprotective effects are primary, direct effects within the CNS or secondary, indirect effects reducing inflammation into the CNS. Although in most neurological disease models the protective effect of estrogen treatment has been shown to be mediated through ER-α and has been associated with anti-inflammatory effects (Merchenthaler et al., 2004; Morales et al., 2006; Suzuki et al., 2006, 2007), these are not mutually exclusive of direct neuroprotective mechanisms. In EAE, ER-α ligand treatment preserved myelin and neuronal staining while reducing inflammation in spinal cords, whereas ER-β ligand treatment preserved myelin and neuronal staining without reducing inflammation (Tiwari-Woodruff et al., 2007). How these two similar, but distinct, neuroprotective treatments might influence the imaging outcomes of gray matter atrophy and diffusion anisotropy is unknown. Thus, the purpose of this study was to contrast the effects of EAE on gray matter atrophy and diffusion anisotropy in ER-α vs. ER-β ligand–treated EAE mice.

MATERIALS AND METHODS

Mice

Female C57BL/6 mice, 6 weeks old, were purchased from the Jackson Laboratory. All studies were performed in accordance with approval from the UCLA Office of Protection of Research Subjects.

Reagents

Estradiol (E2) was purchased from Sigma-Aldrich (St. Louis, MO). Propylpyrazole triol (ER-α ligand) and diarylpropionitrile (ER-β ligand) were purchased from Tocris Bioscience (Ellisville, MO). Miglyol 812 N liquid oil was obtained from Sasol North America (Houston, TX). Myelin oligodendrocyte glycoprotein (MOG) peptide 35–55 was purchased at greater than 98% purity (Chiron Mimotopes, Emeryville, CA).

Animal Protocol

To remove the confound of endogenous circulating estrogens prior to estrogen treatment, female mice were ovariectomized following ketamine (100 mg/kg)/xylazine (10 mg/kg) anesthesia. The fur above the lateral dorsal back was removed and the skin sterilized with betadine and alcohol scrubs. Bilateral incisions were made into the peritoneum. Sutures were placed on the fallopian tubes, and the ovaries were removed. The peritoneal cavity and the abdominal musculature were sutured, and the skin was secured with wound clips. Flunixin meglumine (2.5 mg/kg) was injected s.c. every 12 hr for 2 days for pain. Enrofloxacin was added to the water for 5 days following surgery (45.4 mg/125 ml water). Wound clips were removed 8–10 days following surgery.

The mice were allowed to recuperate for 10 days and then injected every other day with vehicle (10% ethanol and 90% miglyol) alone, E2, ER-α ligand, or ER-β ligand 7 days prior to EAE induction. E2, ER-α ligand, and ER-β ligand were dissolved in vehicle to give the final proper concentration of 0.04 mg/kg/day E2 (Jansson et al., 1994), 10 mg/kg/day ER-α ligand (Harris et al., 2002), and 8 mg/kg/day ER-β ligand (Carswell et al., 2004). E2, ER-α ligand, ER-β ligand, or vehicle alone was given by daily s.c. injections along the midbackline and continued for the entire disease duration (up to 69 days after disease induction).

EAE

Mice were immunized s.c. with MOG peptide 35–55 (300 μg/mouse) and *Mycobacterium tuberculosis* (500 μg/mouse) emulsified in complete Freund's adjuvant, in a volume of 0.1 ml/mouse over two sites: the right-draining inguinal and axillary lymph nodes. One week later a booster immunization was delivered s.c., over the contralateral lymph nodes. Pertussis toxin (500 ng/mouse; List Biological Laboratories, Campbell, CA) was injected intraperitoneally on days 0 and 2 (Suen et al., 1997; Liu et al., 2003). EAE was graded on a scale of 0–5, based on difficulty with ambulation, as described by Pettinelli and McFarlin (1981). Four independent EAE groups were used in this study.

Sample Preparation

Mice were anesthetized deeply using isofluorane. The mouse was then fixed by transcardiac perfusion using 30 ml phosphate-buffered saline (PBS) followed by 30 ml 4% paraformaldehyde (PFA) at 4°C. After death, the head was removed and rocked in 4% PFA overnight at 4°C. Soft tissue was removed, and the skull (containing the brain) was rocked in 50 ml 0.01% sodium azide in PBS for 7.0 days at 4°C. The skull was then transferred to a 5 mM solution of gadoteridol

(Prohance; Bracco Diagnostics, Princeton NJ) and 0.01% sodium azide in PBS and rocked for 15 days at 4°C prior to MRI. Equilibration of the fixed brain in 5 mM gadoteridol solution significantly reduces the T1 of the sample and therefore reduces the total imaging time for a given resolution and target signal-to-noise ratio. All brains were equilibrated at room temperature for 8 hr immediately prior to imaging at 20°C.

MRI

All images were acquired using a vertical-bore 11.7-T Bruker Avance DRX500 system equipped with a Micro2.5 imaging gradient set capable of a peak gradient strength of 1 T/m and a maximum slew rate of 12.5 kT/m/sec. The skull (containing the brain) was secured in a Teflon holder and submerged in a perfluoropolyether (Fomblin; Solvay Solexis, Thorofare, NJ) within a 20-ml vial and imaged using a 35-mm birdcage transmit/receive volume resonator. All samples were equilibrated at room temperature prior to imaging. The ambient bore temperature was maintained at 20°C by thermostatically controlled airflow. Optimized second-order shimming was achieved across the whole sample using the Bruker implementation of Fastmap (Gruetter, 1993).

Diffusion-weighted images were acquired using a conventional pulsed-gradient spin echo (PGSE) sequence (TR/TE = 150 msec/11.6 msec, 256 × 150 × 130 matrix, 19.2 mm × 15 mm × 12 mm FOV, 80 Am isotropic voxel size, 1 average, diffusion gradient length: $\delta = 3$ msec, diffusion gradient separation: $\Delta = 5$ msec, diffusion gradient magnitude: $G_d = 750$ mT/m, nominal b-factor = 1,450 sec/mm^2). An optimized six-point icosahedral encoding scheme (Hasan et al., 2001) was used for diffusion-weighted acquisitions with a single unweighted reference image for a total imaging time of 6 hr.

Image Processing

Image processing was performed using a combination of freely distributed and in-house software implemented in Matlab (The Mathworks, Natick MA). Reconstruction of the diffusion-weighted images included spatial radial Gaussian filtering (radial SD = 0.25 voxel) to smooth the coregistration cost function and improve the SNR of all subsequent calculations. The six diffusion-weighted images were averaged to generate a high-SNR isotropic diffusion-weighted image (iDWI), which could be used for both brain segmentation and image coregistration.

The apparent diffusion tensor was calculated conventionally by inversion of the encoding b-matrix (Mori, 2007). Small shifts and rotations of the diffusion-weighted images were observed and ascribed to residual eddy currents from the high-amplitude diffusion encoding pulses persisting through the echo acquisition. Diffusion-weighted images were consequently registered to the diffusion-unweighted image using a rigid-body transform under the assumption that the original diffusion encoding directions were exact and that the unweighted image best represents the true orientation of the mouse brain relative to the imaging gradient axes. The b-matrix for each diffusion encoding was determined by numerical simulation of the pulse sequence k-space trajectory to account for gradient cross-terms (Mattiello et al., 1997). Eigenvalues, eigenvectors, tensor trace, and FA were calculated conventionally using built-in and custom Matlab functions.

iDWIs were skull-stripped using the Brain Surface Extractor (BSE) within BrainSuite 2 (Shattuck and Leahy, 2001). Inaccuracies were corrected by manually editing the masks using BrainSuite 2. After skull-stripping, field inhomogeneities were corrected using N3 correction (Sled et al., 1998). A minimum deformation target (MDT) was produced as described by Kochunov et al. (2001). Each of the images was then linearly aligned to the MDT with a 12-parameter full-affine transformation using Alignlinear (AIR 5.2.5; Woods et al., 1998a,b) and the least squares with intensity rescaling cost function, followed by a fifth-order polynomial warp using Align_warp (AIR). The images were then resampled and averaged to produce the final minimum deformation atlas (MDA). The MDA was then aligned to a standard atlas (MacKenzie-Graham et al., 2004) to permit the direct comparison of images in a standard space. Automated image processing was performed in the LONI Pipeline Processing Environment (Rex et al., 2003) using an eight-processor Mac Pro computer (Apple, Cupertino, CA).

Anatomical Delineations

A blinded expert neuroanatomist using BrainSuite 2 manually delineated anatomical structures on the MDA. Anatomical delineations included cerebellar cortex, cerebellar white matter, and olfactory bulb. Cerebellar cortex delineations rigorously excluded white matter and partial volume voxels. Anatomical delineations were based on the Mouse Atlas Project 2003 mouse brain atlas (MacKenzie-Graham et al., 2004) and assisted by the *The Mouse Brain in Stereotaxic Coordinates, 3rd ed.* (Franklin and Paxinos, 2008).

Image Analysis

Images were spatially normalized with a 12-parameter full-affine transformation to register each image to the MDA using Alignlinear (AIR). To intensity normalize the images, the alignment was performed with an intensity rescaling cost function. Align_warp (AIR) was used to compute fifth-order polynomial mappings of the MDA to each individual normalized brain. These mappings were then used to warp the anatomical delineations from the MDA to each of the individual images making up the atlas. Individual delineations were manually corrected and volumes recorded in BrainSuite 2. Mean FA measurements were made by averaging the voxel values that were enclosed by the cerebellar white matter delineation using built-in and custom Matlab functions.

Tissue Preparation

After imaging, brains were removed from the skull and prepared for sectioning. Fifty-micrometer-thick sagittal frozen sections were cut using a CM3050S cryostat (Leica Microsystems, Wetzlar, Germany). Free-floating sections were permeabilized in 0.3% Triton X-100 in PBS and blocked with 10% normal goat serum (Vector Laboratories, Burlingame, CA). White matter immunostaining was enhanced by treating sections with 95% ethanol/5% acetic acid for 15 min prior to
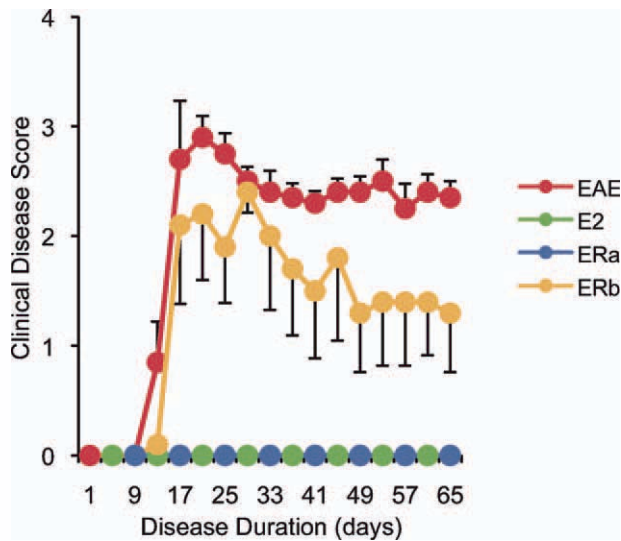
Fig. 1. Clinical disease course. Graph of the mean clinical disease score in mice with EAE plotted against disease duration. Each color represents a treatment group (red for vehicle-treated EAE mice (EAE), green for estradiol-treated EAE mice (E2), blue for ER-α ligand-treated EAE mice (ERa), and yellow for ER-β ligand-treated EAE mice (ERb); for clarity, colors are alternated when lines are overlaid) and are used consistently in subsequent figures. Error bars indicate SEM. [Color figure can be viewed in the online issue, which is available at wileyonlinelibrary.com.]
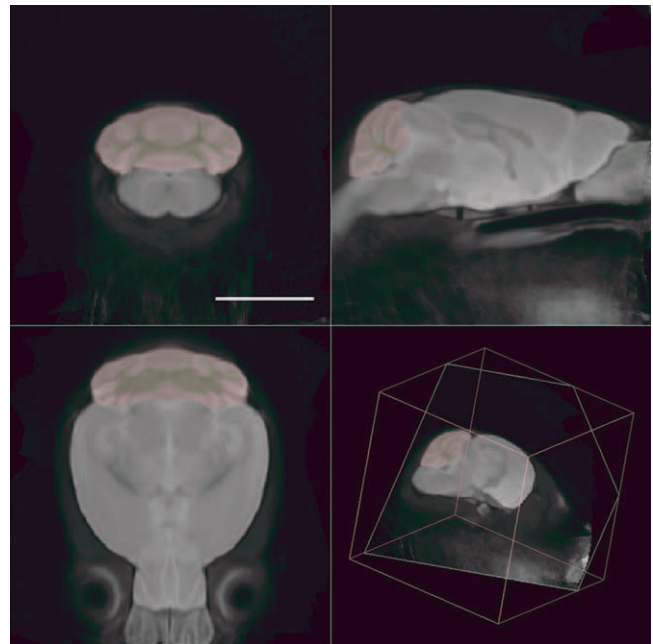

Fig. 2. Minimum deformation atlas and delineations. A minimum deformation atlas was constructed from 30 post-mortem high-resolution isotropic diffusion-weighted images of mouse brain. The anatomical delineations of the cerebellar cortex (red) and cerebellar white matter (yellow) are overlaid on the image. Scale bar = 5 mm. [Color figure can be viewed in the online issue, which is available at wileyonlinelibrary.com.]

permeabilization and blocking. Sections were incubated with primary antibodies in PBS solution containing 2% NGS for 2 hr at room temperature, then overnight at 4°C. The following primary antibodies were used: mouse anti-β-amyloid precursor protein (β-APP; 1:500; Abcam, Cambridge, MA), mouse anti-calbindin-2 (1:500; Sigma-Aldrich), rat anti-CD3 (1:1,000; Millipore, Billerica, MA), rat anti-CD45 (1:1,000; Millipore), rabbit anti-IBA1 (1:1,000; Wako, Richmond, VA), and rat anti-myelin basic protein (MBP; 1:500; Millipore).

Fluorescence secondary antibody labeling included antibodies conjugated to Cy3 and Cy5 (Millipore). To assess the number of cells, 4′,6′-diamidino-2-phenylindole dihydrochloride (DAPI; Invitrogen, Carlsbad, CA) was added for 15 min prior to final washes after secondary antibody addition. The sections were mounted on slides, dried, and coverslipped with fluoromount G (Fisher Scientific, Pittsburgh, PA).

Chromogen immunohistochemistry was performed, after avidin-biotin block, by incubating with a biotinylated secondary antibody. A streptavidin-peroxidase conjugate was added, followed by the addition of 3,3′-diaminobenzidine (DAB; Vector Laboratories). The sections were mounted, dehydrated, and coverslipped with Permount (Fisher Scientific). IgG control experiments were performed for all primary antibodies and no staining was observed under these conditions.

Microscopy and Analysis

Confocal images of immunostained sections were photographed using a spin-disc (Olympus, Center Valley, PA) and TCS-SP laser confocal microscope (Leica Microsystems) with a digital camera (Hamamatsu Photonics, Bridgewater, NJ). All images were collected using similar acquisition parameters. Photomicrographs of each representative experimental group were collected and analyzed in ImageJ (v1.45a).

The degree of axonal damage, demyelination, and inflammation in cerebellar white and gray matter was assessed by quantifying anti-β-APP, anti-MBP, and anti-CD45 staining, respectively, by optical density. Confocal stacks of immunolabeled images from each animal were processed with a series of manual and automated procedures that included the following steps: 1) the images were oriented in the same direction, 2) the RGB channels of the images were split and converted to eight-bit gray images in Image J, 3) gray matter (granule cell, Purkinje cell, and molecular layers) and white matter were manually delineated on the basis of DAPI staining, and 4) threshold gray matter and white matter density was calculated and reported as a percentage of total area.

Macrophages and microglia (IBA-1^{+}), T lymphocytes (CD3^{+}), and Purkinje cells (calbindin-2^{+}) were quantified by counting cell bodies in ×10 images of the entire cerebellum. Dehydration in chromogen-stained sections does not permit many z-planes to be available, so here we counted cells in a projected image. Three to five brain sections (50 μm thick) 200 μm apart were analyzed from each animal (ovarectomized vehicle-treated healthy controls: n = 5; ovarectomized vehicle-treated EAE mice: n = 5; ovarectomized ER-α ligand-treated EAE mice: n = 3; ovarectomized ER-β ligand-treated EAE: n = 4). All sections counted were close to the midline. Only cells with their entire nucleus present in the section

were counted. Some of the animals imaged were excluded from the analysis because of incomplete perfusion or because the tissue was damaged.

Statistical Analysis

All results are presented as mean ± SEM, and statistical differences were determined by the Welch's t-test. ANOVAs and Welch's t-tests were performed in Excel (Microsoft, Redmond, WA). Comparisons were subject to post hoc multiple-comparisons confounds, so the results of the Bonferroni correction ($P < \alpha/n$) were considered.
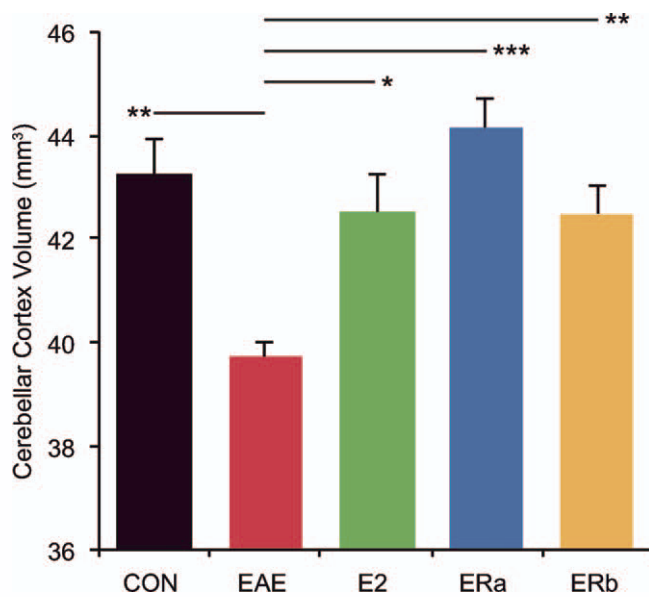

Fig. 3. Estrogen receptor ligand treatment of mice with EAE inhibits atrophy in the cerebellar cortex. Graph of the mean cerebellar cortical volume in ovarectomized vehicle-treated healthy controls (CON), ovarectomized vehicle-treated EAE mice (EAE), ovarectomized estradiol-treated EAE mice (E2), ovarectomized ER-α ligand-treated EAE mice (ERa), and ovarectomized ER-β ligand-treated EAE mice (ERb). Error bars indicate SEM. Asterisks indicate statistical significance ($\star P < 0.01$, $\star\star P < 0.0001$, $\star\star\star P < 0.0001$). All significant differences survive the application of the Bonferroni correction for post hoc testing. [Color figure can be viewed in the online issue, which is available at wileyonlinelibrary.com.]

RESULTS

Post-mortem diffusion tensor imaging (DTI) scans were acquired from 30 female mice: five unmanipulated healthy controls, five ovarectomized vehicle-treated healthy controls, five ovarectomized vehicle-treated EAE mice, five ovarectomized ER-α ligand-treated EAE mice, five ovarectomized ER-β ligand-treated EAE mice, and five ovarectomized E2-treated EAE mice (as a positive control for estrogen treatment). The mice were sacrificed 69 days after disease induction (Fig. 1). There was a significant difference in the disease course between the ER-β ligand-treated EAE mice and both the ER-α ligand- and the E2-treated EAE mice. Specifically, treatment with ER-α ligand and E2 completely blocked the entire disease course at both early and late time points, whereas ER-β ligand treatment ameliorated disease only late, but not early, which is consistent with previous reports (Tiwari-Woodruff et al., 2007; Gold et al., 2009; Tiwari-Woodruff and Voskuhl, 2009).

An MDA was constructed from the 30 isotropic diffusion-weighted images derived from the DT images collected (Fig. 2). The MDA then served as a target space for the spatial and intensity normalization of the original images, correcting both gross size and intensity differences. Following creation of this atlas, the olfactory bulbs, cerebellar cortices, and cerebellar white matter were manually delineated on that atlas. The delineations were then warped onto the normalized images to produce standardized estimates of gray matter volumes in individual subjects.

ER Ligand Treatment of Mice With EAE Inhibits Atrophy in the Cerebellar Cortex

We have previously demonstrated cerebellar atrophy in mice with EAE (MacKenzie-Graham et al., 2006, 2009), an observation that has also been made in MS (Edwards et al., 1999; Iannucci et al., 1999; Liu et al., 1999). Our group has also demonstrated that estrogen-mediated disease protection in EAE may be due not only to the anti-inflammatory effects of estrogen but also to its neuroprotective properties, which can be independent of reducing inflammation (Tiwari-Woodruff et al., 2007; Spence et al., 2011). Specifically, ER-α ligand treatment during EAE ameliorates clinical disease
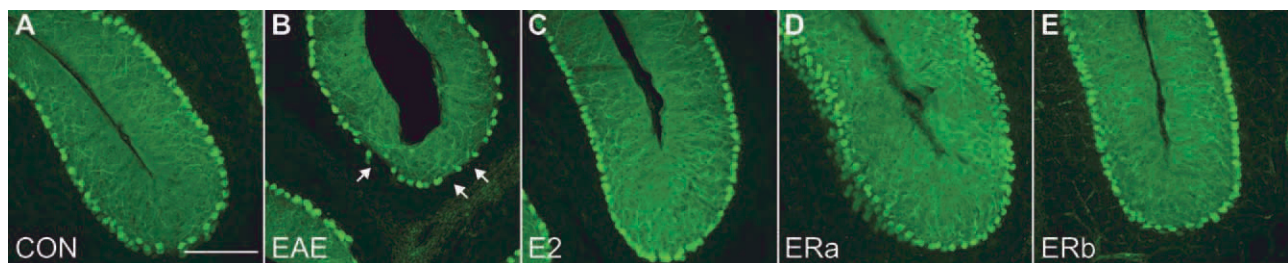

Fig. 4. Purkinje cell staining in the cerebellum. Calbindin-28K immunostained confocal images at 10× magnification from the cerebellum of an ovarectomized vehicle-treated healthy control mouse (A), an ovarectomized vehicle-treated mouse with EAE (B), an ovarectomized E2-treated mouse with EAE (C), an ovarectomized ER-α ligand-treated mouse with EAE (D), and an ovarectomized ER-β ligand-treated mouse with EAE (E). Scale bar = 80 μm. [Color figure can be viewed in the online issue, which is available at wileyonlinelibrary.com.]

while reducing white matter inflammation in spinal cords, whereas ER-β ligand treatment ameliorates clinical disease while not reducing inflammation. Therefore, using the methodology previously described to evaluate gray matter atrophy in mice with EAE (MacKenzie-Graham et al., 2009), we measured cerebellar cortical volumes in EAE mice that had been treated with vehicle, ER-α ligand, or ER-β ligand and compared them
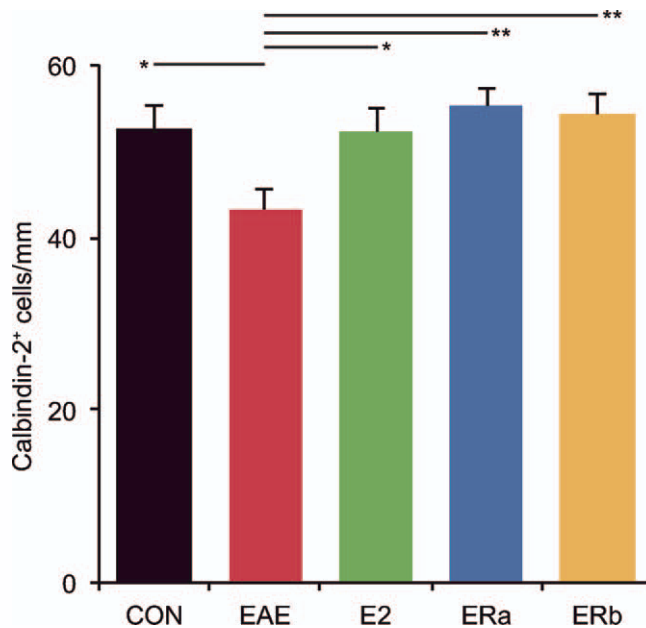

Fig. 5. Estrogen receptor ligand treatment of mice with EAE inhibits Purkinje cell loss. Graph of the number of calbindin-2$^+$ cells in the cerebella of ovarectomized vehicle-treated healthy controls (CON), ovarectomized vehicle-treated EAE mice (EAE), ovarectomized E2-treated EAE mice (E2), ovarectomized ER-α ligand-treated EAE mice (ERa), and ovarectomized ER-β ligand-treated EAE mice (ERb). Error bars indicate SEM. Asterisks indicate statistical significance ($\star P < 0.01$, $\star\star P < 0.001$). All significant differences survive the application of the Bonferroni correction for post hoc testing. [Color figure can be viewed in the online issue, which is available at wileyonlinelibrary.com.]

with healthy controls (Fig. 3). The volumes of the cerebellar cortices in the unmanipulated and ovarectomized healthy controls were not significantly different (data not shown). However, ovarectomized vehicle-treated EAE mice demonstrated an 8.4% decrease in the size of cerebellar cortex compared with ovarectomized vehicle-treated healthy controls ($P = 0.002$). ER-α ligand-treated ($P = 0.00009$), ER-β ligand-treated ($P = 0.003$), or E2-treated ($P = 0.006$) EAE mice had cerebellar cortices that were significantly larger than those of vehicle-treated EAE mice and were not significantly different from those in vehicle-treated healthy controls. The volume of a control structure, the olfactory bulb, did not vary significantly in any of the groups. These data demonstrate that, regardless of whether an estrogen receptor ligand can reduce CNS inflammation, it can prevent cerebellar cortical atrophy in EAE.

ER Ligand Treatment of Mice With EAE Inhibits Purkinje Cell Loss

Our previous work demonstrated cerebellar atrophy in mice with EAE over time (MacKenzie-Graham et al., 2006) and that a loss of Purkinje cells in EAE correlated strongly with that atrophy (MacKenzie-Graham et al., 2009). Furthermore, ER-α expression has been shown in the cerebellum (Simerly et al., 1990; Shughrue et al., 1997), specifically in Purkinje cells (Ikeda and Nagai, 2006), and ER-β has been shown to be expressed in the Purkinje cells (Shughrue et al., 1997; Price and Handa, 2000; Jakab et al., 2001). Thus, we hypothesized that estrogen-mediated disease protection in mice with EAE might be due not only to the effects on inflammation and demyelination but also to the preservation of Purkinje cells in the cerebellum. This may in turn be associated with a prevention of cerebellar atrophy.

Calbindin-2 immunostaining demonstrated a disruption of the normal anatomy of the Purkinje and molecular layers of the cerebellar cortex in vehicle-treated EAE mice compared with E2-treated EAE mice, ER-α ligand-treated EAE mice, ER-β ligand-treated EAE mice, and healthy controls (Fig. 4). Purkinje cell numbers were found to be 17.7% lower in vehicle-treated
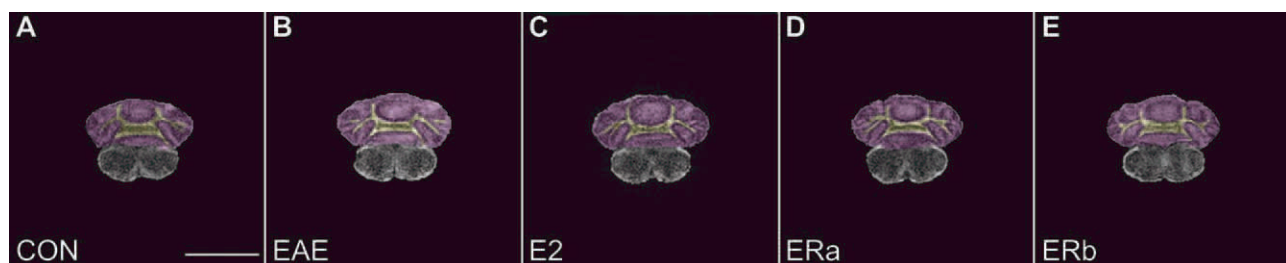

Fig. 6. Fractional anisotropy in the cerebellum. Fractional anisotropy images derived from diffusion tensor images of the cerebellum of an ovarectomized vehicle-treated healthy control mouse (**A**), an ovarectomized vehicle-treated mouse with EAE (**B**), an ovarectomized E2-treated mouse with EAE (**C**), an ovarectomized ER–α ligand-treated mouse with EAE (**D**), and an ovarectomized ER-β ligand-treated mouse with EAE (**E**). The anatomical delineations of the cerebellar cortex (magenta) and cerebellar white matter (yellow) are overlaid on the image. Scale bar = 5 mm. [Color figure can be viewed in the online issue, which is available at wileyonlinelibrary.com.]

EAE mice than in healthy controls ($P = 0.02$; Fig. 5). Purkinje cell numbers were significantly greater in E2 and ER-α ligand-treated EAE mice compared with vehicle-treated EAE mice ($P = 0.02$, $P = 0.002$) and were not significantly different from those in healthy controls. Purkinje cell numbers were also significantly preserved in ER-β ligand-treated EAE mice compared with vehicle-treated EAE mice ($P = 0.004$). Together, these neuroimaging and neuropathological results suggest that gray
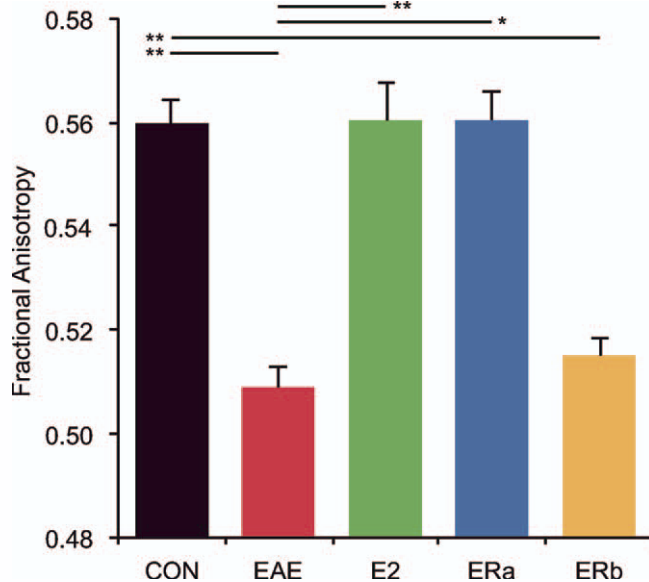

Fig. 7. Fractional anisotropy is reduced in vehicle-treated and ER-β ligand-treated but not in estradiol-treated or ER-α ligand-treated mice with EAE. Graph of the mean fractional anisotropy in the cerebellar white matter of ovarectomized vehicle-treated healthy controls (CON), ovarectomized vehicle-treated EAE mice (EAE), ovarectomized estradiol-treated EAE mice (E2), ovarectomized ER-α ligand-treated EAE mice (ERa), and ovarectomized ER-β ligand-treated EAE mice (ERb). Error bars indicate SEM. Asterisks indicate statistical significance (*$P < 0.01$, **$P < 0.001$). All significant differences survive the application of the Bonferroni correction for post hoc testing. [Color figure can be viewed in the online issue, which is available at wileyonlinelibrary.com.]

matter atrophy as measured by MRI morphometry may be a biomarker for neuronal cell loss in EAE.

FA Is Reduced in Vehicle-Treated and ER-β Ligand-Treated but Not in Estradiol-Treated or ER-α Ligand-Treated Mice With EAE

FA has previously been used as a marker for white matter tract integrity (Werring et al., 1999; Bammer et al., 2000; Filippi et al., 2001). To evaluate white matter tract integrity, we measured the mean FA in the cerebellar white matter of mice with EAE that had been treated with vehicle only, E2, ER-α ligand, or ER-β ligand and compared them with healthy controls (Fig. 6). Vehicle-treated EAE mice demonstrated a 9.1% decrease in the FA of cerebellar white matter compared with controls ($P = 0.00001$). FA was significantly higher in ER-α ligand-treated ($P = 0.00006$) and E2-treated EAE mice ($P = 0.0004$) compared with vehicle-treated EAE mice and was not significantly different from healthy controls (Fig. 7). However, ER-β ligand-treated EAE mice were not significantly different from vehicle-treated EAE mice, demonstrating an 8.0% decrease in FA compared with controls ($P = 0.00004$). Together, these neuroimaging and neuropathological results demonstrate that the treatment effects of atrophy vs. FA may differ during EAE.

ER Ligand Treatment of Mice With EAE Preserves Myelin in the Cerebellum

Changes in FA may be due to changes in myelination, so to investigate further the differences observed in the FA of cerebellar white matter in these mice, we measured myelin basic protein (MBP) expression. MBP immunoreactivity was measured to explore the state of myelin in both white and gray matter in the cerebellum. Healthy control tissue showed dense MBP staining in the central white matter tracts, with regular, parallel arrays of myelinated axons radiating into the granule cell layer (Fig. 8). White matter myelination was substantially greater than gray matter myelination. Quantification indicated that white and gray matter MBP immunoreactivity was significantly lower in vehicle-treated EAE mice than in healthy controls ($P = 0.01$, $P = 0.0004$;

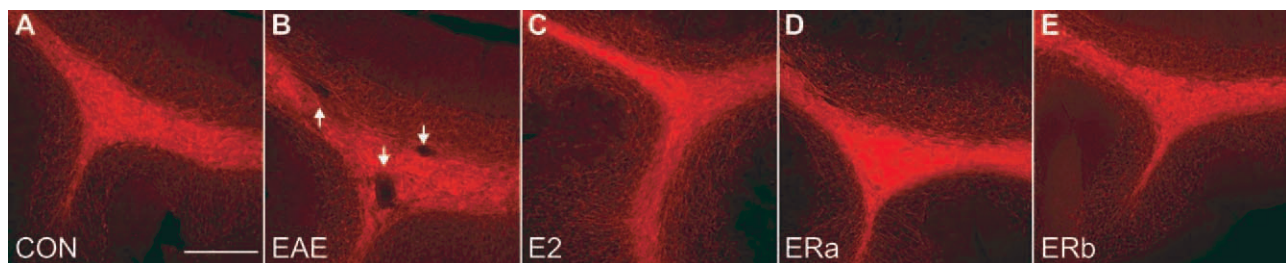Fig. 8. Myelin basic protein staining in the cerebellum. Myelin basic protein immunostained confocal images at 10× magnification from the cerebellum of an ovarectomized vehicle-treated healthy control mouse (A), an ovarectomized vehicle-treated EAE mouse (B), an ovarectomized E2-treated EAE mouse (C), an ovarectomized ER-α ligand-treated EAE mouse (D), and an ovarectomized ER-β ligand-treated EAE mouse (E). Arrows indicate demyelinated lesions. Scale bar = 80 μm. [Color figure can be viewed in the online issue, which is available at wileyonlinelibrary.com.]
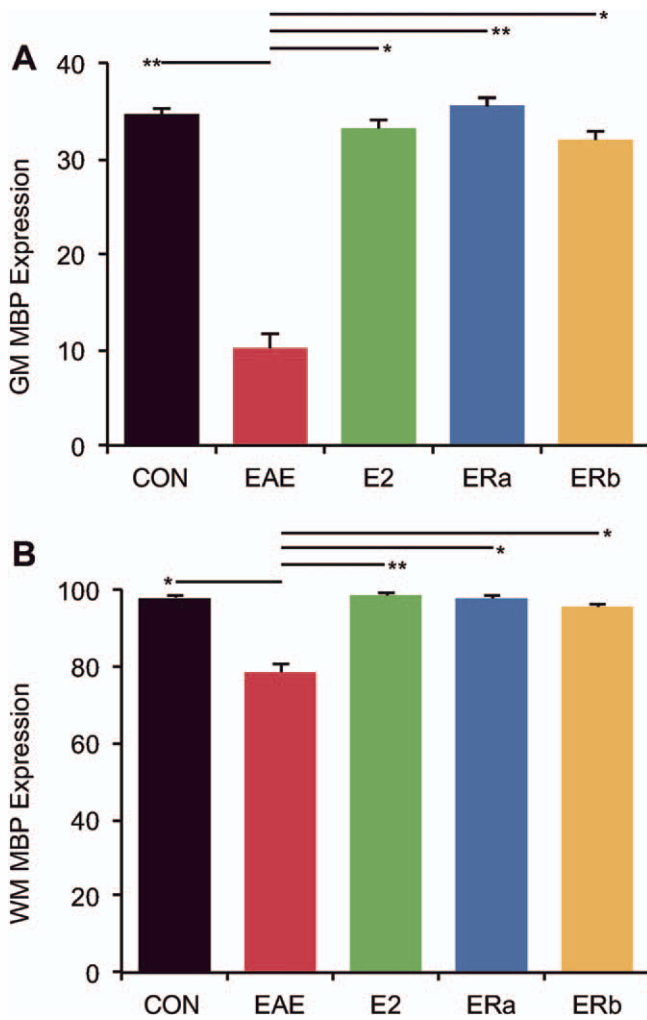
Fig. 9. Estrogen receptor ligand treatment of mice with EAE preserves myelin staining in the cerebellum. **A:** Graph of the mean myelin-staining in the cerebellar white matter of ovarectomized vehicle-treated healthy controls (CON), ovarectomized vehicle-treated EAE mice (EAE), ovarectomized E2-treated EAE mice (E2), ovarectomized ER-α ligand-treated EAE mice (ERa), and ovarectomized ER-β ligand-treated EAE mice (ERb). **B:** Graph of the mean myelin staining in the cerebellar gray matter of ovarectomized vehicle-treated healthy controls (CON), ovarectomized vehicle-treated EAE mice (EAE), ovarectomized E2-treated EAE mice (E2), ovarectomized ER-α ligand-treated EAE mice (ERa), and ovarectomized ER-β ligand-treated EAE mice (ERb). Error bars indicate SEM. Asterisks indicate statistical significance ($\star P < 0.01$, $\star\star P < 0.001$). All significant differences survive the application of the Bonferroni correction for post hoc testing. [Color figure can be viewed in the online issue, which is available at wileyonlinelibrary.com.]

Fig. 9). White and gray matter MBP immunoreactivity was significantly greater in E2-treated EAE mice compared with vehicle-treated EAE mice ($P = 0.0005$, $P = 0.008$) and not significantly different from that in healthy controls. Similarly, white and gray matter MBP immunoreactivity was significantly greater in ER-α ligand-treated EAE mice compared with vehicle-treated

EAE mice ($P = 0.006$, $P = 0.0006$) and not significantly different from that in healthy controls. Interestingly, white and gray matter MBP immunoreactivity was also significantly preserved in ER-β ligand-treated EAE mice compared with vehicle-treated EAE mice ($P = 0.01$, $P = 0.006$). The preservation of myelin staining in ER-β ligand-treated mice that had a significant decrease in FA suggested that a neuropathology other than demyelination underlay the decrease in FA.

Cerebellar Inflammation in EAE Is Decreased With ER-α Ligand but Not in ER-β Ligand Treatment

Previous studies have shown that changes in FA can be caused not only by demyelination but also by inflammation. Thus, we next focussed our neuropathological analysis of the cerebella of mice with EAE on inflammation. Protein tyrosine phosphatase, receptor type C (CD45) immunoreactivity is a commonly used measure of inflammation. Therefore, CD45 immunoreactivity was measured to explore the state of inflammation in both white and gray matter in the cerebellum. Healthy control tissue showed very little CD45 staining in either the white or the gray matter (Fig. 10). Quantification indicated that white and gray matter CD45 immunoreactivity was significantly higher in vehicle-treated EAE mice compared with healthy controls ($P = 0.00005$, $P = 0.001$; Fig. 11A,B). White and gray matter CD45 immunoreactivity was significantly decreased in E2-treated compared with vehicle-treated EAE mice ($P = 0.001$, $P = 0.00002$) and was not significantly different from that of healthy controls. Similarly, white and gray matter CD45 immunoreactivity was significantly decreased in ER-α ligand-treated compared with vehicle-treated EAE mice ($P = 0.001$, $P = 0.00002$) and not significantly different from that in healthy controls. In contrast, ER-β ligand-treated EAE mice were not significantly different from vehicle-treated EAE mice and demonstrated a significant increase in white and gray matter CD45 immunoreactivity compared with healthy controls ($P = 0.0001$, $P = 0.0001$).

To characterize the inflammatory response better, we next stained with antibodies to ionized calcium binding adaptor molecule 1 (IBA1) and T-cell coreceptor (CD3). Anti-IBA1 stains cells of the macrophage/microglia lineage whereas anti-CD3 stains T lymphocytes. IBA1^{+} cell numbers were significantly higher in vehicle-treated EAE mice than in healthy controls in both white and gray matter ($P = 0.000003$, $P = 0.00004$; Fig. 11C,D). IBA1^{+} cell numbers in white and gray matter were significantly lower in E2-treated EAE mice compared with vehicle-treated EAE mice ($P = 0.000003$, $P = 0.00004$) and not significantly different from those of healthy controls. Similarly, IBA1^{+} cell numbers in white and gray matter were significantly lower in ER-α ligand-treated EAE mice compared with vehicle-treated EAE mice ($P = 0.000003$, $P = 0.00003$) and not significantly different from those of healthy controls. In contrast, ER-β ligand-treated EAE mice were not significantly different
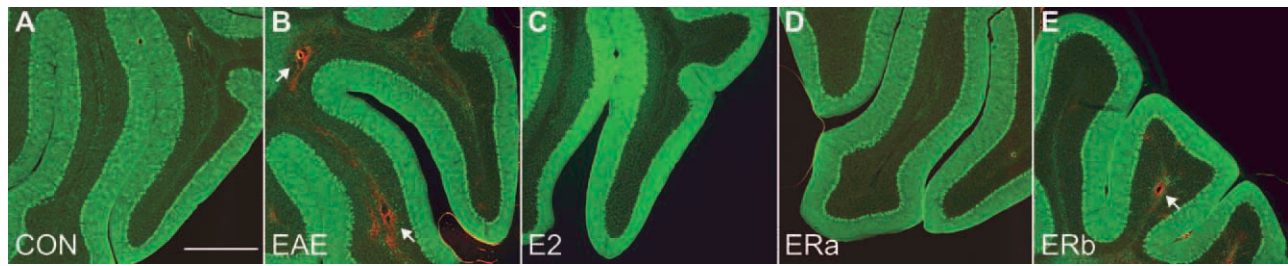
Fig. 10. Inflammatory cell staining in the cerebellum. CD45-immunostained confocal images at 4× magnification from the cerebellum of an ovarectomized vehicle-treated healthy control mouse (**A**), an ovarectomized vehicle-treated EAE mouse (**B**), an ovarectomized E2-treated EAE mouse (**C**), an ovarectomized ER-α ligand-treated EAE mouse (**D**), and an ovarectomized ER-β ligand-treated EAE mouse (**E**). Arrows indicate cellular infiltrate. Scale bar = 200 μm. [Color figure can be viewed in the online issue, which is available at wileyonlinelibrary.com.]

from vehicle-treated EAE mice and demonstrated significantly greater IBA1$^+$ cell numbers compared with controls ($P = 0.000002$, $P = 0.00004$).

Quantification of CD3$^+$ staining indicated that T-lymphocyte numbers in white and gray matter were significantly higher in vehicle-treated EAE mice than in healthy controls ($P = 0.000005$, $P = 0.00001$; Fig. 11E,F). CD3$^+$ cell numbers in white and gray matter were significantly lower in E2-treated EAE mice compared with vehicle-treated EAE mice ($P = 0.000005$, $P = 0.00003$) and not significantly different from those of controls. Similarly, CD3$^+$ cell numbers in white and gray matter were significantly lower in ER-α ligand-treated EAE mice compared with vehicle-treated EAE mice ($P = 0.000005$, $P = 0.00003$) and not significantly different from those of controls. However, ER-β ligand-treated EAE mice were not significantly different from vehicle-treated EAE mice and demonstrated significantly higher CD3$^+$ cell numbers compared with controls ($P = 0.000003$, $P = 0.00001$). There was no significant difference in CD3$^+$ cell number between vehicle-treated and ER-β ligand-treated EAE mice.

Estrogen Receptor Ligand Treatment of Mice With EAE Abrogates Axonal Damage in Cerebellar White Matter

Another possible cause for changes in FA is axonal damage. Therefore, we measured β-APP expression, a sensitive marker of axonal injury (Ferguson et al., 1997). Healthy control tissue showed virtually no β-APP staining in white matter tracts (Fig. 12). Quantification indicated that β-APP immunoreactivity was much higher in vehicle-treated EAE mice than healthy controls ($P = 0.0001$; Fig. 13). β-APP immunoreactivity was significantly lower in E2- and ER-α ligand-treated EAE mice compared with vehicle-treated EAE mice ($P = 0.0001$, $P = 0.0001$). Interestingly, β-APP immunoreactivity was also significantly lower in ER-β ligand-treated EAE mice compared with vehicle-treated EAE mice ($P = 0.0002$).

Together, these neuroimaging and neuropathological results demonstrate that the ability of a given treatment to reduce inflammation in a given substructure coincides with its ability to preserve FA within the same substructure in EAE. These results are summarized in Table I.

DISCUSSION

Most therapies for MS have been developed to reduce inflammation. Interferon-β, glatiramer acetate, and mitoxantrone have considerably improved the therapeutic options for patients with MS. These anti-inflammatory agents reduce relapse rates and reduce the appearance of contrast-enhancing lesions. However, their efficacy in preventing accumulation of disability and slowing gray matter atrophy and their impact on disease progression have been somewhat disappointing (Trojano et al., 2006; Van der Walt et al., 2010).

Here we have contrasted the effects of treatment with ER-α vs. ER-β ligands on gray matter atrophy in EAE, the MS model with a known pathogenic role for both inflammation and neurodegeneration. Morphometry demonstrated that atrophy was abrogated in ER-α ligand-, ER-β ligand-, and E2-treated EAE mice. Similarly, Purkinje cell numbers were preserved in ER-α ligand-, ER-β ligand-, and E2-treated EAE mice. Interestingly, the mean FA was preserved in ER-α ligand- and E2-treated EAE mice but not in ER-β ligand-treated EAE mice. Immunohistochemistry demonstrated that white and gray matter myelin staining was preserved in ER-α ligand-, ER-β ligand-, and E2-treated EAE mice; however, cerebellar inflammation in EAE was decreased in ER-α ligand- and E2-treated, but not in ER-β ligand-treated EAE mice. Overall, we have demonstrated that DTI can visualize treatment effects on different elements of the pathology of EAE. Specifically, atrophy is a biomarker for Purkinje cell number, and FA can be used as a biomarker for inflammation in the cerebellum in EAE. Both proved to be be highly informative in assessing the effects of treatments on disease.

Because the variability was low in both clinical scores and mean cerebellar cortex volumes within each treatment group, one could not assess whether mice with worse clinical scores had more atrophy within a given treatment group. However, between-group comparisons revealed that vehicle-treated mice with EAE
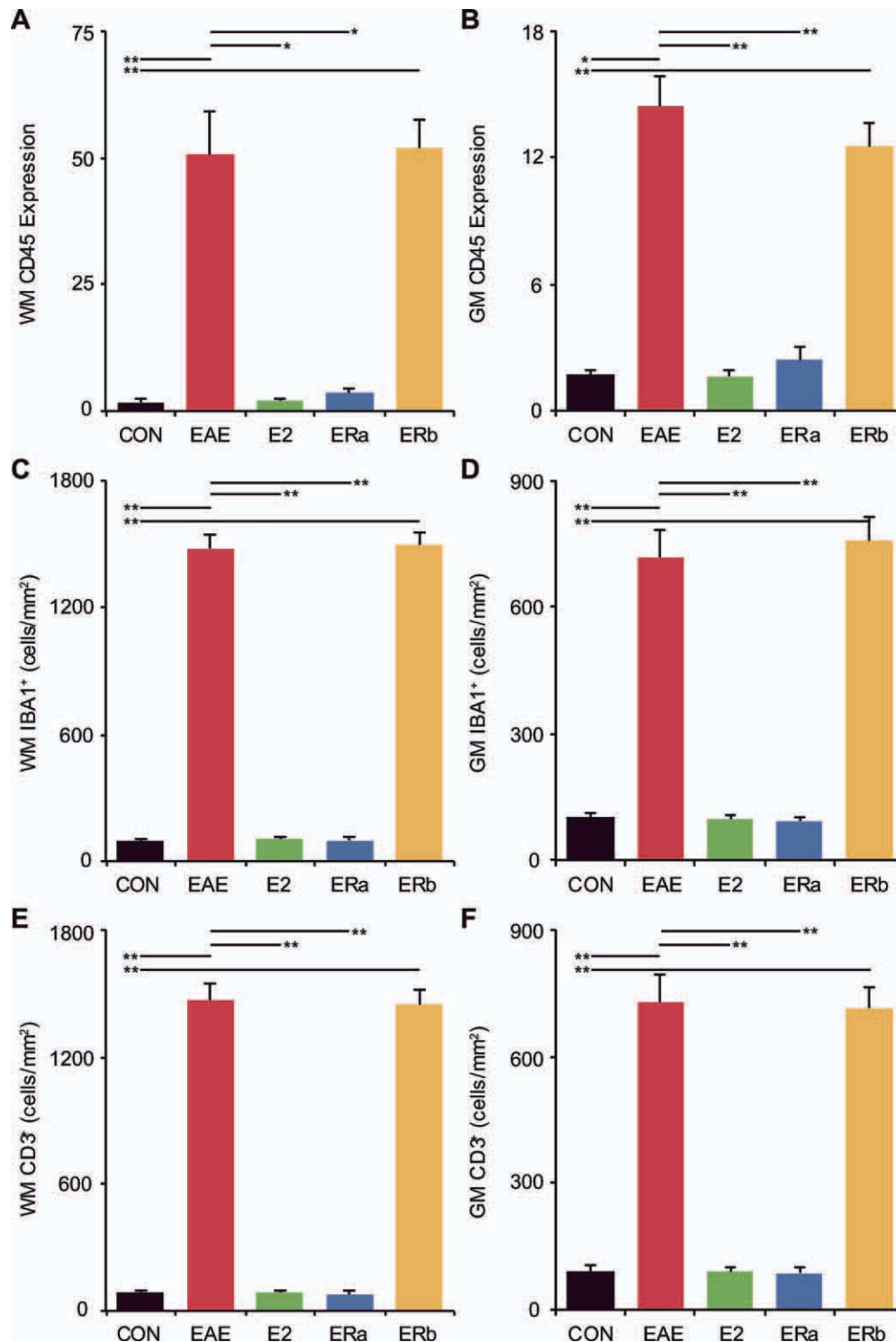
Fig. 11. Inflammation is increased in vehicle-treated and ER-β ligand-treated but not in ER-α ligand-treated mice with EAE. **A:** Graph of the mean CD45 staining in the cerebellar gray matter of ovarectomized vehicle-treated healthy controls (CON), ovarectomized vehicle-treated EAE mice (EAE), ovarectomized E2-treated EAE mice (E2), ovarectomized ER-α ligand-treated EAE mice (ERa), and ovarectomized ER-β ligand-treated EAE mice (ERb). **B:** Graph of the mean CD45 staining in the cerebellar white matter of ovarectomized vehicle-treated healthy controls, ovarectomized vehicle-treated EAE mice, ovarectomized E2-treated EAE mice, ovarectomized ER-α ligand-treated EAE mice, and ovarectomized ER-β ligand-treated EAE mice. **C:** Graph of the mean number of IBA1+ cells per square millimeter in the cerebellar white matter of ovarectomized vehicle-treated healthy controls, ovarectomized vehicle-treated EAE mice, ovarectomized E2-treated EAE mice, ovarectomized ER-α ligand-treated EAE mice, and ovarectomized ER-β ligand-treated EAE mice. **D:** Graph of the number of IBA1+ cells per square millimeter in the cerebellar gray matter of ovarectomized vehicle-treated healthy con-trols, ovarectomized vehicle-treated EAE mice, ovarectomized E2-treated EAE mice, ovarectomized ER-α ligand-treated EAE mice, and ovarectomized ER-β ligand-treated EAE mice. **E:** Graph of the mean number of CD3+ cells per square millimeter in the cerebellar white matter of ovarectomized vehicle-treated healthy controls, ovarectomized vehicle-treated EAE mice, ovarectomized E2-treated EAE mice, ovarectomized ER-α ligand-treated EAE mice, and ovarectomized ER-β ligand-treated EAE mice. **F:** Graph of the number of CD3+ cells per square millimeter in the cerebellar gray matter of ovarectomized vehicle-treated healthy controls, ovarectomized vehicle-treated EAE mice, ovarectomized E2-treated EAE mice, ovarectomized ER-α ligand-treated EAE mice, and ovarectomized ER-β ligand-treated EAE mice. Error bars indicate SEM. Asterisks indicate statistical significance ($\star P < 0.01$, $\star\star P < 0.001$). All significant differences survive the application of the Bonferroni correction for post hoc testing. [Color figure can be viewed in the online issue, which is available at wileyonlinelibrary.com.]
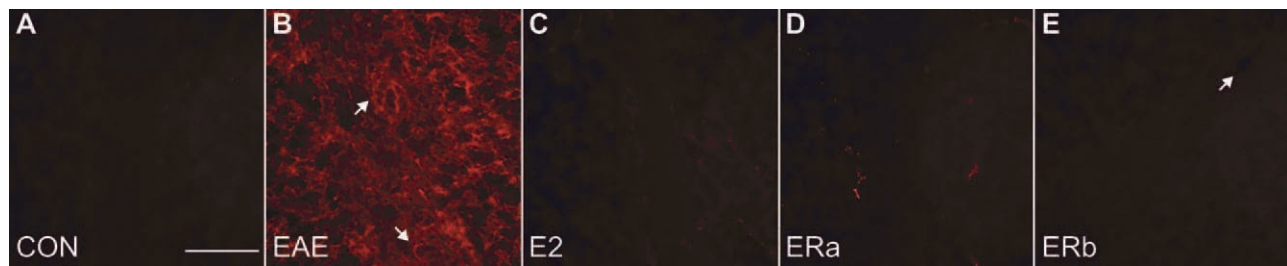
Fig. 12. β-Amyloid precursor protein staining in the cerebellum. β-APP (red)-immunostained confocal images at ×40 from the cerebellum of an ovarectomized vehicle-treated healthy control mouse (**A**), an ovarectomized vehicle-treated EAE mouse (**B**), an ovarectomized E2-treated EAE mouse (**C**), an ovarectomized ER-α ligand-treated EAE mouse (**D**), and an ovarectomized ER-β ligand-treated EAE mouse (**E**). Arrows in B indicate lesions centered on blood vessels, whereas the arrow in E indicates a blood vessel without a surrounding lesion. Scale bar = 20 μm. [Color figure can be viewed in the online issue, which is available at wileyonlinelibrary.com.]
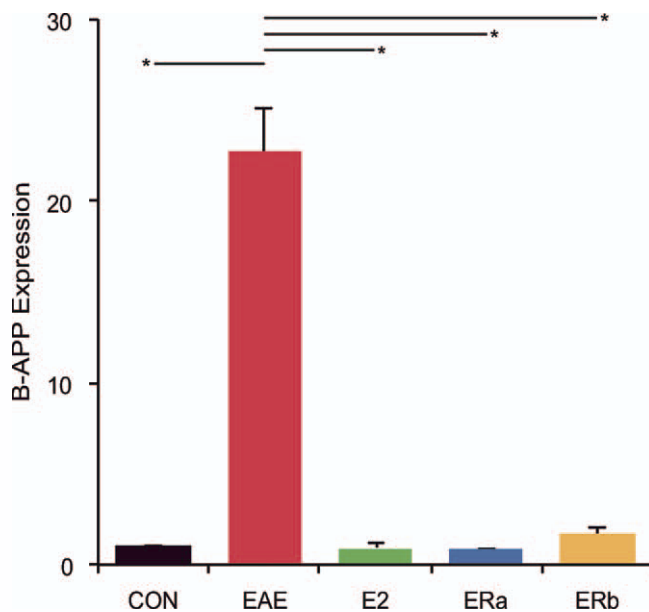

Fig. 13. Estrogen receptor ligand treatment of mice with EAE abrogates β-amyloid precursor protein staining in the cerebellum. Graph of the mean β-APP staining in the cerebellar white matter of ovarectomized vehicle-treated healthy controls (CON), ovarectomized vehicle-treated EAE mice (EAE), ovarectomized E2-treated EAE mice (E2), ovarectomized ER-α ligand-treated EAE mice (ERa), and ovarectomized ER-β ligand-treated EAE mice (ERb). Error bars indicate SEM. Asterisks indicate statistical significance ($\star P < 0.0005$). All significant differences survive the application of the Bonferroni correction for post hoc testing. [Color figure can be viewed in the online issue, which is available at wileyonlinelibrary.com.]

indeed had both worse clinical scores and more atrophy than E2-, ER-α ligand-, or ER-β ligand-treated mice with EAE. FA values were also characterized by low variability within groups. In contrast to cerebellar volumes, between-group comparisons of cerebellar FA did not show an association with disease. This was principally a result of the fact that the ER-β ligand-treated group demonstrated disease amelioration paired with a low FA.

Our results show for the first time that estrogen treatment can prevent gray matter atrophy and preserve Purkinje cells in the cerebellum during EAE. The prevention of the loss of this major neuronal cell type in EAE is significant because of the cells' functional relevance. Purkinje cells are intimately involved in motor activity and represent the only output pathway of the cerebellar cortex (Parent, 1996). The ER-β ligand treatment effect was clearly not mediated by a reduction of cerebellar inflammation, because there was no significant difference in CD45 expression, IBA1$^+$ cell number, or CD3$^+$ cell number between ER-β ligand-treated and vehicle-treated EAE mice. What remains unknown is whether the neuroprotective effect of ER-β ligand treatment is mediated through binding to ER-β receptors on neurons, oligodendrocytes, or astrocytes, because all of these CNS cell types have been shown to express ER-β in vivo (Platania et al., 2003). In fact, it is likely that there is a direct effect of estrogen receptor β ligand treatment on Purkinje cell survival, because Purkinje cells have been shown to express ER-β (Shughrue et al., 1997; Price and Handa, 2000; Jakab et al., 2001; Sakamoto et al., 2003).

Although our results are strongly suggestive of a direct effect of estrogen on Purkinje cells, we cannot eliminate the possibility that the estrogen effect is mediated by other cells such as astrocytes (Spence et al., 2011) or even non-CNS cells. Propyl pyrazole triol (ER-α ligand) and diarylpropionitrile (ER-β ligand) are ER agonists with well characterized affinities for ER-α and ER-β respectively (Meyers et al., 2001; Harrington et al., 2003), and previous studies with knockout mice (Morales et al., 2006) have established the selectivity and responsiveness of these ligands in vivo. Results obtained from this approach should complement studies with knockout mice and help to expand our appreciation of the complexities of estrogen's action.

A decrease in FA has previously been reported in dysmyelinating shiverer mice compared with normal controls, suggesting that FA is indicative of the level of myelination (Tyszka et al., 2006). Our finding that the FA is decreased in mice with EAE was similarly reported by authors using a related measure, relative anisotropy in

TABLE I. Summary of Imaging and Histology Results [mean (SEM)]

	CON	EAE	E2	ERa	ERb
Volumetry	43.2 (0.7)	39.7 (0.3)	42.5 (0.5)	44.2 (0.6)	42.5 (0.7)
Fractional anisotropy	0.560 (0.005)	0.509 (0.004)	0.560 (0.007)	0.561 (0.006)	0.515 (0.003)
Purkinje Cell Number	52.6 (2.8)	43.3 (2.4)	52.2 (2.8)	55.2 (2.2)	54.3 (2.3)
MBP GM	34.53 (0.68)	10.19 (1.44)	33.12 (1.01)	35.68 (0.90)	31.95 (0.78)
MBP WM	97.95 (0.37)	78.61 (2.06)	98.35 (0.76)	97.52 (1.12)	95.2 (1.04)
CD45 GM	1.7 (0.3)	14.4 (1.4)	1.6 (0.3)	2.4 (0.6)	12.5 (1.2)
CD45 WM	1.7 (0.5)	50.7 (8.4)	2.0 (0.2)	3.5 (1.0)	52.0 (5.6)
IBA1 GM	102.0 (8.9)	718.6 (63.8)	97.6 (9.5)	93.6 (8.9)	757.2 (56.1)
IBA1 WM	94.0 (12.8)	1,481.2 (67.8)	102.4 (12.2)	98.8 (11.8)	1,497.8 (61.8)
CD3 GM	89.6 (13.8)	729.6 (63.8)	89.8 (9.2)	87.6 (11.4)	716.2 (48.6)
CD3 WM	82.4 (12.4)	1,470.0 (76.5)	87.6 (9.5)	78.0 (12.8)	1,449.0 (65.7)
β-APP	1.0 (0.1)	22.7 (2.4)	0.9 (0.2)	0.8 (0.1)	1.6 (0.5)

EAE (Budde et al., 2009). Consistent with our results, in which decreases in FA were independent of myelin staining, Budde et al. (2009) found no correlation between relative anisotropy and MBP staining in EAE. Differences between these two reports involve the relationship between FA and inflammation. Budde et al. demonstrated a weak correlation between relative anisotropy and cellular infiltrate. In contrast, our findings suggested that decreases in FA are related to inflammation, insofar as both vehicle- and ER-β ligand-treated EAE mice demonstrated a decrease in FA, and both vehicle- and ER-β ligand-treated EAE mice demonstrated increased inflammatory cell infiltration. One possible explanation for the discrepancy in our findings is differences in staining. We stained for very specific markers of inflammation (CD45, CD3, and IBA1), whereas Budde et al. used a nonspecific nuclear stain (DAPI$^+$) to measure inflammation indirectly. Perhaps more importantly, we evaluated FA in the cerebellar white matter, whereas Budde et al. evaluated white matter tracts of the spinal cord. The diffusion anisotropy in the cerebellar white matter is lower than in the white matter tracts of the spinal cord in normals. The cerebellar white matter contains many white matter tracts traveling in different directions; it comprises the cerebellodentatorubral, cerebellodentatothallamic, cerebellovestibular, cuneocerebellar, olivocerebellar, pontocerebellar, reticulcerebellar, spinocerebellar, trigeminocerebellar, and vestibulospinal fiber tracts, not to mention the myelinated Purkinje cell axons that project to the deep cerebellar nuclei. It is possible that the FA in the white matter in the cerebellum is more sensitive to inflammation than in the highly organized spinal cord. Finally, we calculated the mean FA for the entire cerebellar white matter and counted infiltrating cells across the entire cerebellum, whereas Budde et al. focussed on specific areas of the spinal cord and evaluated their correlations on a pixel-by-pixel basis. Together these findings suggest that FA may be a sensitive biomarker for inflammation depending on the CNS area of study.

In an effort to understand better the pathology in MS lesions, DTI has proved to be a valuable tool. Anisotropy measures have commonly been used as biomarkers for demyelination and axonal damage. For example, decreased FA has been shown to be more pronounced in lesions than in the normal-appearing white matter (NAWM); although its values are highly heterogeneous. This has been interpreted as indicating the variable degrees of tissue damage occurring within MS lesions (Filippi et al., 2001). However, FA is always lower in contrast-enhancing lesions, especially ring-enhancing lesions (Bammer et al., 2000), compared with nonenhancing lesions, the latter of which are thought to reflect demyelination and axonal damage with minimal inflammatory infiltrate (Filippi et al., 2001; Castriota-Scanderbeg et al., 2003). Contrast enhancement is thought to be due to blood–brain barrier breakdown secondary to inflammatory cell infiltration. Histological studies lend support to this idea, demonstrating that lesions with enhancement show inflammatory activity, either macrophage infiltration (Nesbit et al., 1991) or perivascular lymphocytic infiltration (Katz et al., 1993). Our findings demonstrate that inflammation can play an important role in the decrease of FA in the white matter of mice with EAE and suggest that the use of decreased FA as a biomarker for demyelination and axonal damage (Hesseltine et al., 2006) should be tempered with the understanding that inflammation may be playing a major role in the observed decrease.

In summary, we have found that treatment of mice with EAE with either ER-α or ER-β ligand prevents gray matter atrophy and preserves a major neuronal population. This finding has implications for treatment in MS, suggesting that early treatment with neuroprotective agents might help spare patients from permanent clinical disability and irreversible neuronal damage. Furthermore, multimodal approaches using neuroimaging combined with immunohistochemistry in disease models suggests that DTI can indeed differentiate between different treatment mechanisms.

REFERENCES

Amato MP, Portaccio E, Stromillo ML, Goretti B, Zipoli V, Siracusa G, Battaglini M, Giorgio A, Bartolozzi ML, Guidi L, Sorbi S, Federico A, De Stefano N. 2008. Cognitive assessment and quantitative magnetic resonance metrics can help to identify benign multiple sclerosis. Neurology 71:632–638.

Bammer R, Augustin M, Strasser-Fuchs S, Seifert T, Kapeller P, Stollberger R, Ebner F, Hartung HP, Fazekas F. 2000. Magnetic resonance

diffusion tensor imaging for characterizing diffuse and focal white matter abnormalities in multiple sclerosis. Magn Reson Med 44:583–591.

Bebo BF Jr, Fyfe-Johnson A, Adlard K, Beam AG, Vandenbark AA, Offner H. 2001. Low-dose estrogen therapy ameliorates experimental autoimmune encephalomyelitis in two different inbred mouse strains. J Immunol 166:2080–2089.

Bermel RA, Bakshi R. 2006. The measurement and clinical relevance of brain atrophy in multiple sclerosis. Lancet Neurol 5:158–170.

Birk K, Ford C, Smeltzer S, Ryan D, Miller R, Rudick RA. 1990. The clinical course of multiple sclerosis during pregnancy and the puerperium. Arch Neurol 47:738–742.

Budde MD, Xie M, Cross AH, Song SK. 2009. Axial diffusivity is the primary correlate of axonal injury in the experimental autoimmune encephalomyelitis spinal cord: a quantitative pixelwise analysis. J Neurosci 29:2805–2813.

Calabrese M, Mattisi I, Rinaldi F, Favaretto A, Atzori M, Bernardi V, Barachino L, Romualdi C, Rinaldi L, Perini P, Gallo P. 2010. Magnetic resonance evidence of cerebellar cortical pathology in multiple sclerosis. J Neurol Neurosurg Psychiatry 81:401–404.

Camicioli R, Moore MM, Kinney A, Corbridge E, Glassberg K, Kaye JA. 2003. Parkinson's disease is associated with hippocampal atrophy. Mov Disord 18:784–790.

Carswell HV, Macrae IM, Gallagher L, Harrop E, Horsburgh KJ. 2004. Neuroprotection by a selective estrogen receptor β agonist in a mouse model of global ischemia. Am J Physiol Heart Circ Physiol 287:H1501–H1504.

Castriota-Scanderbeg A, Fasano F, Hagberg G, Nocentini U, Filippi M, Caltagirone C. 2003. Coefficient D(av) is more sensitive than fractional anisotropy in monitoring progression of irreversible tissue damage in focal nonactive multiple sclerosis lesions. AJNR Am J Neuroradiol 24:663–670.

Chard DT, Griffin CM, Parker GJ, Kapoor R, Thompson AJ, Miller DH. 2002. Brain atrophy in clinically early relapsing-remitting multiple sclerosis. Brain 125:327–337.

Confavreux C, Hutchinson M, Hours MM, Cortinovis-Tourniaire P, Moreau T. 1998. Rate of pregnancy-related relapse in multiple sclerosis. Pregnancy in Multiple Sclerosis Group [see comments]. N Engl J Med 339:285–291.

Crawford DK, Mangiardi M, Song B, Patel R, Du S, Sofroniew MV, Voskuhl RR, Tiwari-Woodruff SK. 2010. Oestrogen receptor β ligand: a novel treatment to enhance endogenous functional remyelination. Brain 133:2999–3016.

Edwards SG, Gong QY, Liu C, Zvartau ME, Jaspan T, Roberts N, Blumhardt LD. 1999. Infratentorial atrophy on magnetic resonance imaging and disability in multiple sclerosis. Brain 122:291–301.

Ferguson B, Matyszak MK, Esiri MM, Perry VH. 1997. Axonal damage in acute multiple sclerosis lesions. Brain 120:393–399.

Filippi M, Cercignani M, Inglese M, Horsfield MA, Comi G. 2001. Diffusion tensor magnetic resonance imaging in multiple sclerosis. Neurology 56:304–311.

Firbank MJ, Blamire AM, Krishnan MS, Teodorczuk A, English P, Gholkar A, Harrison R, O'Brien JT. 2007. Atrophy is associated with posterior cingulate white matter disruption in dementia with Lewy bodies and Alzheimer's disease. Neuroimage 36:1–7.

Fisher E, Rudick RA, Simon JH, Cutter G, Baier M, Lee JC, Miller D, Weinstock-Guttman B, Mass MK, Dougherty DS, Simonian NA. 2002. Eight-year follow-up study of brain atrophy in patients with MS. Neurology 59:1412–1420.

Franklin KBJ, Paxinos G. 2008. The mouse brain in stereotaxic coordinates. New York: Academic Press.

Ge Y, Grossman RI, Udupa JK, Wei L, Mannon LJ, Polansky M, Kolson DL. 2000. Brain atrophy in relapsing-remitting multiple sclerosis and secondary progressive multiple sclerosis: longitudinal quantitative analysis. Radiology 214:665–670.

Gold SM, Sasidhar MV, Morales LB, Du S, Sicotte NL, Tiwari-Woodruff SK, Voskuhl RR. 2009. Estrogen treatment decreases matrix metalloproteinase (MMP)-9 in autoimmune demyelinating disease through estrogen receptor α (ERα). Lab Invest 89:1076–1083.

Gruetter R. 1993. Automatic, localized in vivo adjustment of all first- and second-order shim coils. Magn Reson Med 29:804–811.

Harrington WR, Sheng S, Barnett DH, Petz LN, Katzenellenbogen JA, Katzenellenbogen BS. 2003. Activities of estrogen receptor α- and β-selective ligands at diverse estrogen responsive gene sites mediating transactivation or transrepression. Mol Cell Endocrinol 206:13–22.

Harris HA, Katzenellenbogen JA, Katzenellenbogen BS. 2002. Characterization of the biological roles of the estrogen receptors, ERα and ERβ, in estrogen target tissues in vivo through the use of an ERα-selective ligand. Endocrinology 143:4172–4177.

Hasan KM, Parker DL, Alexander AL. 2001. Comparison of gradient encoding schemes for diffusion-tensor MRI. J Magn Reson Imaging 13:769–780.

Hesseltine SM, Law M, Babb J, Rad M, Lopez S, Ge Y, Johnson G, Grossman RI. 2006. Diffusion tensor imaging in multiple sclerosis: assessment of regional differences in the axial plane within normal-appearing cervical spinal cord. AJNR Am J Neuroradiol 27:1189–1193.

Iannucci G, Minicucci L, Rodegher M, Sormani MP, Comi G, Filippi M. 1999. Correlations between clinical and MRI involvement in multiple sclerosis: assessment using T(1), T(2) and MT histograms. J Neurol Sci 171:121–129.

Ikeda Y, Nagai A. 2006. Differential expression of the estrogen receptors α and β during postnatal development of the rat cerebellum. Brain Res 1083:39–49.

Ito A, Bebo BF Jr, Matejuk A, Zamora A, Silverman M, Fyfe-Johnson A, Offner H. 2001. Estrogen treatment down-regulates TNF-α production and reduces the severity of experimental autoimmune encephalomyelitis in cytokine knockout mice. J Immunol 167:542–552.

Jakab RL, Wong JK, Belcher SM. 2001. Estrogen receptor β immunoreactivity in differentiating cells of the developing rat cerebellum. J Comp Neurol 430:396–409.

Jansson L, Olsson T, Holmdahl R. 1994. Estrogen induces a potent suppression of experimental autoimmune encephalomyelitis and collagen-induced arthritis in mice. J Neuroimmunol 53:203–207.

Katz D, Taubenberger JK, Cannella B, McFarlin DE, Raine CS, McFarland HF. 1993. Correlation between magnetic resonance imaging findings and lesion development in chronic, active multiple sclerosis. Ann Neurol 34:661–669.

Kim S, Liva SM, Dalal MA, Verity MA, Voskuhl RR. 1999. Estriol ameliorates autoimmune demyelinating disease: implications for multiple sclerosis. Neurology 52:1230–1238.

Kochunov P, Lancaster JL, Thompson P, Woods R, Mazziotta J, Hardies J, Fox P. 2001. Regional spatial normalization: toward an optimal target. J Comput Assist Tomogr 25:805–816.

Liu C, Edwards S, Gong Q, Roberts N, Blumhardt LD. 1999. Three dimensional MRI estimates of brain and spinal cord atrophy in multiple sclerosis. J Neurol Neurosurg Psychiatry 66:323–330.

Liu HB, Loo KK, Palaszynski K, Ashouri J, Lubahn DB, Voskuhl RR. 2003. Estrogen receptor α mediates estrogen's immune protection in autoimmune disease. J Immunol 171:6936–6940.

MacKenzie-Graham A, Lee EF, Dinov ID, Bota M, Shattuck DW, Ruffins S, Yuan H, Konstantinidis F, Pitiot A, Ding Y, Hu G, Jacobs RE, Toga AW. 2004. A multimodal, multidimensional atlas of the C57BL/6J mouse brain. J Anat 204:93–102.

MacKenzie-Graham A, Tinsley MR, Shah KP, Aguilar C, Strickland LV, Boline J, Martin M, Morales L, Shattuck DW, Jacobs RE, Voskuhl RR, Toga AW. 2006. Cerebellar cortical atrophy in experimental autoimmune encephalomyelitis. Neuroimage 32:1016–1023.

MacKenzie-Graham A, Tiwari-Woodruff SK, Sharma G, Aguilar C, Vo KT, Strickland LV, Morales L, Fubara B, Martin M, Jacobs RE, Johnson GA, Toga AW, Voskuhl RR. 2009. Purkinje cell loss in experimental autoimmune encephalomyelitis. Neuroimage 48:637–651.

Mattiello J, Basser PJ, Le Bihan D. 1997. The b matrix in diffusion tensor echo-planar imaging. Magn Reson Med 37:292–300.

Merchenthaler I, Lane MV, Numan S, Dellovade TL. 2004. Distribution of estrogen receptor α and β in the mouse central nervous system: in vivo autoradiographic and immunocytochemical analyses. J Comp Neurol 473:270–291.

Meyers MJ, Sun J, Carlson KE, Marriner GA, Katzenellenbogen BS, Katzenellenbogen JA. 2001. Estrogen receptor-β potency-selective ligands: structure-activity relationship studies of diarylpropionitriles and their acetylene and polar analogues. J Med Chem 44:4230–4251.

Morales LB, Loo KK, Liu HB, Peterson C, Tiwari-Woodruff S, Voskuhl RR. 2006. Treatment with an estrogen receptor α ligand is neuroprotective in experimental autoimmune encephalomyelitis. J Neurosci 26:6823–6833.

Mori S. 2007. Introduction to diffusion tensor imaging. Amsterdam: Elsevier.

Nesbit GM, Forbes GS, Scheithauer BW, Okazaki H, Rodriguez M. 1991. Multiple sclerosis: histopathologic and MR and/or CT correlation in 37 cases at biopsy and three cases at autopsy. Radiology 180:467–474.

Palaszynski KM, Liu H, Loo KK, Voskuhl RR. 2004. Estriol treatment ameliorates disease in males with experimental autoimmune encephalomyelitis: implications for multiple sclerosis. J Neuroimmunol 149:84–89.

Papenfuss TL, Powell ND, McClain MA, Bedarf A, Singh A, Gienapp IE, Shawler T, Whitacre CC. 2011. Estriol generates tolerogenic dendritic cells in vivo that protect against autoimmunity. J Immunol 186:3346–3355.

Parent A. 1996. Carpenter's human neuroanatomy. Media, PA: Williams & Wilkins.

Pettinelli CB, McFarlin DE. 1981. Adoptive transfer of experimental allergic encephalomyelitis in SJL/J mice after in vitro activation of lymph node cells by myelin basic protein: requirement for Lyt1$^+$2$^-$ T lymphocytes. J Immunol 127:1420–1423.

Pierpaoli C, Basser PJ. 1996. Toward a quantitative assessment of diffusion anisotropy. Magn Reson Med 36:893–906.

Platania P, Laureanti F, Bellomo M, Giuffrida R, Giuffrida-Stella AM, Catania MV, Sortino MA. 2003. Differential expression of estrogen receptors α and β in the spinal cord during postnatal development: localization in glial cells. Neuroendocrinology 77:334–340.

Polanczyk MJ, Carson BD, Subramanian S, Afentoulis M, Vandenbark AA, Ziegler SF, Offner H. 2004. Cutting edge: estrogen drives expansion of the CD4$^+$CD25$^+$ regulatory T cell compartment. J Immunol 173:2227–2230.

Price RH Jr, Handa RJ. 2000. Expression of estrogen receptor-β protein and mRNA in the cerebellum of the rat. Neurosci Lett 288:115–118.

Rex DE, Ma JQ, Toga AW. 2003. The LONI Pipeline Processing Environment. Neuroimage 19:1033–1048.

Rudick RA, Fisher E, Lee JC, Simon J, Jacobs L. 1999. Use of the brain parenchymal fraction to measure whole brain atrophy in relapsing-remitting MS. Multiple Sclerosis Collaborative Research Group. Neurology 53:1698–1704.

Sakamoto H, Mezaki Y, Shikimi H, Ukena K, Tsutsui K. 2003. Dendritic growth and spine formation in response to estrogen in the developing Purkinje cell. Endocrinology 144:4466–4477.

Shattuck DW, Leahy RM. 2001. Automated graph-based analysis and correction of cortical volume topology. IEEE Trans Med Imaging 20:1167–1177.

Shughrue PJ, Lane MV, Merchenthaler I. 1997. Comparative distribution of estrogen receptor-α and -β mRNA in the rat central nervous system. J Comp Neurol 388:507–525.

Simerly RB, Chang C, Muramatsu M, Swanson LW. 1990. Distribution of androgen and estrogen receptor mRNA-containing cells in the rat brain: an in situ hybridization study. J Comp Neurol 294:76–95.

Skare S, Li T, Nordell B, Ingvar M. 2000. Noise considerations in the determination of diffusion tensor anisotropy. Magn Reson Imaging 18:659–669.

Sled JG, Zijdenbos AP, Evans AC. 1998. A nonparametric method for automatic correction of intensity nonuniformity in MRI data. IEEE Trans Med Imaging 17:87–97.

Song SK, Sun SW, Ju WK, Lin SJ, Cross AH, Neufeld AH. 2003. Diffusion tensor imaging detects and differentiates axon and myelin degeneration in mouse optic nerve after retinal ischemia. Neuroimage 20:1714–1722.

Spence RD, Hamby ME, Umeda E, Itoh N, Du S, Wisdom AJ, Cao Y, Bondar G, Lam J, Ao Y, Sandoval F, Suriany S, Sofroniew MV, Voskuhl RR. 2011. Neuroprotection mediated through estrogen receptor-α in astrocytes. Proc Natl Acad Sci U S A 108:8867–8872.

Subramanian S, Matejuk A, Zamora A, Vandenbark AA, Offner H. 2003. Oral feeding with ethinyl estradiol suppresses and treats experimental autoimmune encephalomyelitis in SJL mice and inhibits the recruitment of inflammatory cells into the central nervous system. J Immunol 170:1548–1555.

Suen WE, Bergman CM, Hjelmstrom P, Ruddle NH. 1997. A critical role for lymphotoxin in experimental allergic encephalomyelitis. J Exp Med 186:1233–1240.

Suzuki S, Brown CM, Wise PM. 2006. Mechanisms of neuroprotection by estrogen. Endocrine 29:209–215.

Suzuki S, Brown CM, Dela Cruz CD, Yang E, Bridwell DA, Wise PM. 2007. Timing of estrogen therapy after ovariectomy dictates the efficacy of its neuroprotective and antiinflammatory actions. Proc Natl Acad Sci U S A 104:6013–6018.

Tiwari-Woodruff S, Voskuhl RR. 2009. Neuroprotective and antiinflammatory effects of estrogen receptor ligand treatment in mice. J Neurol Sci 286:81–85.

Tiwari-Woodruff S, Morales LB, Lee R, Voskuhl RR. 2007. Differential neuroprotective and antiinflammatory effects of estrogen receptor (ER)α and ERβ ligand treatment. Proc Natl Acad Sci U S A 104:14813–14818.

Trojano M, Russo P, Fuiani A, Paolicelli D, Di Monte E, Granieri E, Rosati G, Savettieri G, Comi G, Livrea P, Group MS. 2006. The Italian Multiple Sclerosis Database Network (MSDN): the risk of worsening according to IFNβ exposure in multiple sclerosis. Mult Scler 12:578–585.

Tyszka JM, Readhead C, Bearer EL, Pautler RG, Jacobs RE. 2006. Statistical diffusion tensor histology reveals regional dysmyelination effects in the shiverer mouse mutant. Neuroimage 29:1058–1065.

van den Elskamp IJ, Boden B, Dattola V, Knol DL, Filippi M, Kappos L, Fazekas F, Wagner K, Pohl C, Sandbrink R, Polman CH, Uitdehaag BM, Barkhof F. 2010. Cerebral atrophy as outcome measure in short-term phase 2 clinical trials in multiple sclerosis. Neuroradiology 52:875–881.

Van der Walt A, Butzkueven H, Kolbe S, Marriott M, Alexandrou E, Gresle M, Egan G, Kilpatrick T. 2010. Neuroprotection in multiple sclerosis: a therapeutic challenge for the next decade. Pharmacol Ther 126:82–93.

Voskuhl RR. 2003. Hormone-based therapies in MS. Int MS J 10:60–66.

Weiss DJ, Gurpide E. 1988. Non-genomic effects of estrogens and anti-estrogens. J Steroid Biochem 31:671–676.

Werring DJ, Clark CA, Barker GJ, Thompson AJ, Miller DH. 1999. Diffusion tensor imaging of lesions and normal-appearing white matter in multiple sclerosis. Neurology 52:1626–1632.

Woods RP, Grafton ST, Holmes CJ, Cherry SR, Mazziotta JC. 1998a. Automated image registration: I. General methods and intrasubject, intramodality validation. J Comput Assist Tomogr V22:139–152.

Woods RP, Grafton ST, Watson JD, Sicotte NL, Mazziotta JC. 1998b. Automated image registration: II. Intersubject validation of linear and nonlinear models. J Comput Assist Tomogr 22:153–165.

Zang YC, Halder JB, Hong J, Rivera VM, Zhang JZ. 2002. Regulatory effects of estriol on T cell migration and cytokine profile: inhibition of transcription factor NF-kappa B. J Neuroimmunol 124:106–114.